RSC Advances

PAPER

View Article Online
View Journal | View Issue

Cite this: *RSC Adv.*, 2025, **15**, 31609

Excellent hydrogen storage capabilities and optoelectronic attributes of $XClH_6$ (Li, Na, and K) perovskite hydrides for green energy technologies

Hudabia Murtaza,[a] Ahmed B. M. Ibrahim,[b] Junaid Munir,[c] Abhinav Kumar,[d] Mohamed A. Habib,[b] Ankit Dilipkumar Oza[e] and Quratul Ain *[a]

The high hydrogen storage capacity, stability, and reversibility of perovskite hydrides make them promising materials for the energy industry. They play a vital role in sustainable energy technologies, including fuel cells and hydrogen storage systems. This work offers a comprehensive understanding of the physical attributes of $XClH_6$ (X = Li, Na, and K), utilizing the DFT-based Wien2K code. The quantum mechanical effects, along with Coulombic repulsions, are incorporated using the mBJ functional. For the assessment of the structural and thermo-dynamical integrity of $XClH_6$ (X = Li, Na, and K), optimization curves, tolerance factors, and formation energies are evaluated. The second ordered stress energy tensor is employed to compute the elastic constants of cubic $XClH_6$ (X = Li, Na, and K). The electronic properties are analyzed, which revealed indirect bandgaps of 0.29 eV, 0.55 eV, and 1.87 eV for $LiClH_6$, $NaClH_6$, and $KClH_6$, respectively. The electromagnetic interaction depicts that the studied hydrides possess higher divergence and dispersion in the visible range. The gravimetric densities for $LiClH_6$, $NaClH_6$, and $KClH_6$ are obtained as 10.97 wt%, 8.38 wt%, and 6.92 wt%, respectively, which exceed the criteria mentioned by the US DOE for 2025, making these materials excellent contenders for renewable energy and hydrogen storage.

Received 20th May 2025
Accepted 14th August 2025

DOI: 10.1039/d5ra03544a

rsc.li/rsc-advances

Introduction

As the global economy expands swiftly and the population grows steadily, the demand for energy is rising at an unmatched rate.[1,2] Security and energy concerns due to heavy fossil fuel consumption have become significant global challenges in recent years.[3,4] The excessive usage of energy generated *via* fossil fuels has immensely contributed towards harmful gas emissions.[5] CO_2 emissions have significantly impacted forestry and agriculture, which has increased global warming. Renewable energy sources are crucial to the global decarbonization strategy that intends to reduce carbon emissions.[6] Lately, researchers and engineers have been vigorously trying to generate efficient renewable energy devices that are environmentally friendly, and among these sources, hydrogen energy has become a popular research topic.[7] Hydrogen is a light element, and the energy generated through its burning does not emit greenhouse gases, which makes hydrogen energy an effective and inexpensive energy source.[8] Hydrogen energy is currently receiving a lot of interest because of its high energy density, cleanliness, and renewability. Hydrogen is commonly stored by compression, liquefaction, and other processes. However, these traditional treatments are costly and pose possible safety risks. As a result, it is critical to select appropriate compounds as hydrogen storage materials.[9] Hydrogen has emerged as a viable alternative energy source in the last ten years, providing a long-term way to reach carbon neutrality and deal with the world's energy dilemma. The entire hydrogen energy cycle produces minimal carbon emissions, and its large reserve provides a long-term and reliable supply.[10,11] For safe and effective hydrogen energy storage systems, particularly in automotive technologies, solid-state materials have shown immense potential.[12] Through chemisorption and physisorption processes, solid-state materials make it possible to store hydrogen, and when compared with conventional hydrogen storage systems, these approaches have shown increased reversibility, safety, and storage capacity.[13] Despite the use of standard hydrogen storage materials in hydrogen energy systems, achieving large storage capacity and ensuring safe conveyance remain a challenge. As a result, the quest for new hydrogen storage materials has risen to the top of the hydrogen energy research agenda. Notably, perovskite hydrides stand out as interesting possibilities because of their large hydrogen storage capacity and stable architectures.[14] With the chemical formula ABH_3, perovskite hydrides are becoming increasingly recognized

[a]*Department of Physics, University of Management and Technology, Lahore, Pakistan. E-mail: ainnie357@yahoo.com*
[b]*Department of Chemistry, College of Science, Imam Mohammad Ibn Saud Islamic University (IMSIU), Riyadh 11623, Saudi Arabia*
[c]*Department of Physics, Riphah International University, Lahore, Pakistan*
[d]*Centre for Research Impact & Outcome, Chitkara University Institute of Engineering and Technology, Chitkara University, Rajpura, 140401, Punjab, India*
[e]*University Centre for Research and Development, Chandigarh University, Mohali, Punjab, 140413, India*

as a distinct family of materials. High hydrogen storage capacity, good volumetric and gravimetric densities, a broad range of compositional options, strong structural stability, and simple synthesis techniques are what make them appealing.[15] Various studies including carbon-based porous materials,[16,17] liquid hydrogen storage in cryogenic tanks[18] and solid-state storage in metal hydrides[19] have been reported in the literature. One of the major properties that distinguishes perovskite compounds for H_2 storage is their ability to adsorb H_2.[20] Hydride perovskites commonly have gravimetric densities between 1.2 and 6.0 wt%.[21] Perovskite hydrides, such as $XPtH_3$(X = Rb, K, Na, and Li),[22] KXH_3 (X = Mg and Be),[23] $AMgH_3$ (A = Be and Ca),[24] $XAlH_3$ (X = K and Na),[25] $XScH_3$ (X = K and Na),[26] $XSnH_3$ (X = K and Li),[27] $XMnH_3$ (X = K and Li),[28] $XCrH_3$ (X = Na and K),[29] $CsZH_3$ (Z = Mn and Cr),[30] $XLiH_3$ (X = Mg, Ca, Sr, and Ba),[31] Na_2CaCdH_6,[32] Cs_2TlXH_6 (X = In and Ga),[33] and BFe_2MgH (B = Be, Mg, and Ca),[34] are reported to have a significant gravimetric ratio, which makes these perovskites a viable option for hydrogen-based applications. The advancement in the field of hydrogen energy relies on developing novel materials that can adsorb hydrogen effectively. Furthermore, it is also crucial for the newly developed novel materials to adhere to the US DOE criteria for hydrogen storage. To achieve this purpose, we conducted first-principles research on the hydrogen storage potential of alkali-based $XClH_6$ (X = Li, Na, and K) hydrides and investigated their storage performance and physical qualities, which provided valuable information for future experimental development. These hydrides are not theoretically and experimentally explored prior to this research but their possible synthesis path can be inferred from related hydrides and complex hydrides, which are already discussed in the literature. Approaches like solid-state reactions or high-pressure synthesis methods, in which excess hydrogen is reacted with the equivalent alkali metal chlorides (LiCl, NaCl, and KCl) in the presence of a metal catalyst (such as Ni-, Pd-, or Ti-based) at high pressures and temperatures, could be one conceivable path. The synthesis of $LiAlH_4$ and $NaBH_4$ complex hydrides has been accomplished using these techniques. One additional strategy to create novel hydrides is through ball milling. Our findings advance hydrogen storage technology, aligning with the US Department of Energy's aim to exceed current performance standards and accelerate the transition to maintainable energy.

Research methodology

The Wien2K code is utilized to assess the physical features of $XClH_6$ (X = Li, Na, and K). Wien2K is a DFT-based code, and it is one of the most effective codes to assess the electronic properties of complex materials.[35] This code employs the FP-LAPW technique to resolve the Kohn–Sham equations. The Kohn–Sham equations are a set of self-consistent equations derived within the density functional theory to describe the ground-state electron density of a many-body system. They replace the complex many-electron problem with a simpler system of non-interacting electrons moving in an effective potential. The FP-LAPW technique divides the space into non-overlapping atomic spheres and an interstitial region, which enables precise calculations for complex materials.[36] The combined quantum mechanical interactions of electrons and coulombic interactions for $XClH_6$ (X = Li, Na, and K) are treated *via* the mBJ approximation. The mBJ approximation is stated as

$$V_X^{mBJ}(r) = cV_X^{BR}(r) + (3c-2)\frac{1}{\pi}\sqrt{\frac{5}{12}}\sqrt{\frac{2t(r)}{\rho(r)}} \quad (1)$$

Here $V_X^{BR}(r)$ is the Becke Russell's potential and c is given as:

$$c = \alpha + \beta\left(\frac{1}{V_{cell}}\int\frac{\nabla\rho(r)}{\rho(r)}\right)^{\frac{1}{2}} \quad (2)$$

In the above-mentioned equation, $\frac{\nabla\rho(r)}{\rho(r)}$ represents the ratio of the electron density, V_{cell} is the unit cell volume and "α" and "β" are Wien2K parameters, which can be adjusted according to the desired calculation.[37] For accuracy and precision in the computed results, the plane-wave cut-off was controlled using the parameter RMT × K_{max} = 7.0, ensuring well-converged total energies, whereas L_{max} and G_{max} are set as 11 and 20 $(a.u)^{-1}$. The cut-off energy is selected as −7 Ryd, which aided in preventing the charge leakage from the muffin-tin region. The muffin-tin radii are selected as "Li = 2.5 $(a.u)^{-1}$", "K = 2.44 $(a.u)^{-1}$", "Na = 2.09 $(a.u)^{-1}$", "Cl = 1.56 $(a.u)^{-1}$" and "H = 0.79 $(a.u)^{-1}$". A Monkhorst–Pack mesh of 13 × 13 × 13 was used, resulting in a total of 1900 irreducible k-points in the Brillouin zone. The structural properties for $XClH_6$ (X = Li, Na, and K) are analyzed using the PBE-GGA functional, and the optimized lattice parameters are obtained through Birch's Murnaghan curve fitting. The hydrogen storage potential is measured *via* gravimetric and volumetric densities, whereas hydrogen desorption is analyzed by using the Gibb's free energy. To understand the atomic positions and bond lengths for the studied hydrides, the VESTA software is used.[38] The elastic constants were calculated using the Thomas–Charpin strain–stress method, where small finite deformations (typically 0.5–1%) were applied to the equilibrium structure. The resulting stress tensors were computed and fitted to Hooke's law. The optical relations derived from the Kramer–Kronig equations are utilized to assess the electromagnetic interactions of the studied hydride.

Results and discussion

Structural properties

To determine whether the material is suitable for hydrogen storage, its structural qualities must be investigated. For perovskite hydrides, it is essential to assess the material's capacity to endure repeated hydrogenation and dehydrogenation cycles without significant structural damage. This provides the material's stability and resilience under cyclic loading, which are key considerations in ensuring the long-term usage and efficiency as a hydrogen storage medium.[39] $XClH_6$ (X = Li, Na, and K) possesses the general formula of ABH_6, where the A-site is occupied by alkali metals, *i.e.*, Li, Na, and K, and the B-site is occupied by Cl. The Wyckoff atomic positions for alkali earth metals are obtained as (1/4, 1/4, 1/4), the halide atom is placed at (0, 0, 1/2), and the hydrogen atom is placed at (0, 0,

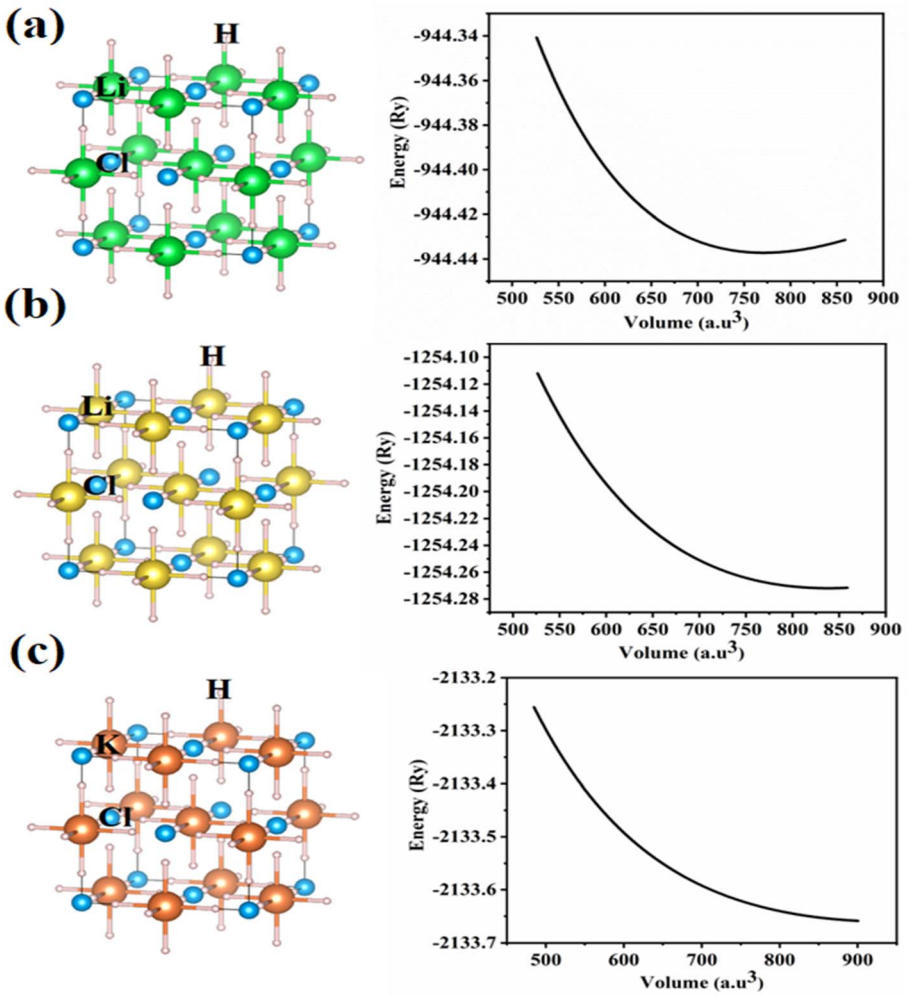

Fig. 1 Crystal structures and optimization results for (a) $LiClH_6$, (b) $NaClH_6$ and (c) $KClH_6$.

0.241). The atomic bond lengths for Na–H, K–H, Cl–H, and Li–H are observed as 4.39 Å, 3.16 Å, 2.23 Å, and 2.10 Å. Fig. 1 reports the crystal structures and optimization curves for $LiClH_6$, $NaClH_6$, and $KClH_6$. With the assistance of the volume optimization curves of the studied hydrides, we have obtained the ground state energies. These ground state energies indicate the structural stability of the hydrides under study, allowing for additional computational research to determine their suitability for optoelectronics and hydrogen storage. The Birch's equation is employed to analyze the relaxed parameters for $LiClH_6$, $NaClH_6$, and $KClH_6$. The equation is stated as

$$E(V) = E_0 + \frac{9V_0B_0}{16}\left\{\left[\left(\frac{V}{V_0}\right)^{\frac{2}{3}} - 1\right]^3 B_0' + \left[\left(\frac{V}{V_0}\right)^{\frac{2}{3}} - 1\right]^2 \left[6 - 4\left(\frac{V}{V_0}\right)^{\frac{2}{3}}\right]\right\} \quad (3)$$

The relaxed, optimized parameters for $LiClH_6$, $NaClH_6$, and $KClH_6$ are described in Table 1. From the obtained ground state energies, it is noticed that among all the studied hydrides, $KClH_6$ is the most stable hydride. The material's capacity to maintain its phase and characteristics under particular temperature and pressure conditions without changing on its own is known as thermodynamic stability. Formation energies are computed to assess the thermodynamic stability of $XClH_6$ (X = Li, Na, and K). The energy change that follows when a compound is produced from its component elements is measured by the formation energy. A positive value denotes instability since energy input is necessary for the compound's creation, whereas a negative value suggests stability because energy is released during formation. The formation energies for the studied hydrides are analyzed using the following equation:

$$E_F = E_{Total} - \left(E_{Na/Li/K} + E_{Cl} + \frac{6}{2}E_H\right) \quad (4)$$

The total energies for the studied hydrides are mentioned in Table 1. The individual energies for Li, Na, K, Cl, and H are mentioned as E_{Na}, E_{Li}, E_K, E_{Cl}, and E_H. From the obtained

Table 1 Relaxed parameters for $XClH_6$ (X = Li, Na, and K)

Perovskites	$LiClH_6$	$NaClH_6$	$KClH_6$
$a = b = c$ (Å)	7.702	7.934	8.289
Symmetry	Cubic		
Space group	*Fm3m*-225		
B (GPa)	22.5	19.30	13.32
B' (GPa)	3.38	3.18	4.55
V_o (a.u^3)	770.99	840.54	900.92
E_o (R_y)	−944.43	−1254.27	−2133.71
E_F (eV per atom)	−4.35	−3.73	−3.61
τ	0.92	0.91	0.89

formation energies, it is noted that $LiClH_6$, $NaClH_6$, and $KClH_6$ are stable, corresponding to their constituent atoms.

A crucial notion in comprehending the structural reliability of perovskite materials is the tolerance factor. It shows how effectively the components' ionic sizes mesh to create a stable crystal structure. A cubic perovskite structure, which is also stable, has a tolerance factor equal to one, whereas deviations could result in distortions or other phases, such as orthorhombic or tetragonal. The optimal tolerance factor for cubic perovskites usually falls between 0.8 and 1.0.[40] Values within this range ensure that the ions can occupy their lattice locations without substantial strain. Phase transitions or structural instability are frequently seen in materials with tolerance factors outside of this range. The studied hydrides exhibit tolerance factor values in the optimal range between 0.8 and 1, which implies that our studied hydrides are stable and can hold cubic formation at room temperature.

Solid state hydrogen storage

Hydrogen energy is a flexible energy source that can be utilized in power generation, fuel cells, and industrial applications. For hydrogen to be used in an effective way, it must be stored safely and effectively. The efficiency of a substance or system in storing hydrogen gas is usually indicated by its hydrogen storage capacity.[41] To compute the hydrogen storage capacities for $LiClH_6$, $NaClH_6$ and $KClH_6$, we first analyze the gravimetric ratio, which is determined as:

$$C_{wt\%} = \left(\frac{(H/m)M_H}{M_{Host} + (H/m)M_H} \times 100\right)\% \quad (5)$$

For the studied hydrides, the total molar mass is depicted as "M_{Host}", the molar mass of hydrogen is presented as "M_H", whereas the ratio of the total number of hydrogen atoms present in the material is mentioned as "(H/m)". The evaluated gravimetric density values for $XClH_6$ (X = Li, Na, and K) are listed in Table 2. The computed gravimetric densities for the studied hydrides exceed the US DOE criteria for hydrides, which demonstrate their potential as effective materials for storing hydrogen. The studied hydrides are tempting for energy storage applications because of their capacity to store a substantial amount of hydrogen per unit mass. Their high gravimetric capacity indicates that they are suitable for use in automobile and portable hydrogen storage systems. The graphical representations for the gravimetric densities for $LiClH_6$, $NaClH_6$ and $KClH_6$ are depicted in Fig. 2(a). Another important factor to take into account when evaluating a material's ability to hold hydrogen is the hydrogen desorption temperature. It is the amount of thermal heat needed to eliminate the hydrogen from the material. Two crucial parameters required to ascertain the desorption temperature are the hydrogen entropy value, which is 130.7 J mol^{-1} K^{-1}, and the material formation energy value. Desorption temperature is evaluated as $T_d = E_F/\Delta S$.

The US DOE defines the desorption temperature range for perovskite hydrides as 233 K and 333 K [68]. Our calculated desorption temperatures are higher than the suggested range, which indicates the possibility of a trade-off between desorption ease and storage stability. Higher temperatures could make storage safer, but they could also make it more difficult to release hydrogen in an energy-efficient manner. Graphical illustrations for desorption temperatures for $LiClH_6$, $NaClH_6$, and $KClH_6$ are depicted in Fig. 2(b). Lastly, we have also computed the volumetric storage capacity for $XClH_6$ (X = Li, Na, and K) using $\rho\left(\frac{gH_2}{L}\right) = \frac{N_H M_H}{V(\mathring{A})^3}$.

According to the findings, the volumetric density follows the order of $LiClH_6$ > $NaClH_6$ > KClH6. This trend is observed due to the decreasing molecular weights and compactness of the materials. Among the studied hydrides, $LiClH_6$ is the lightest, which implies that it possesses a higher tendency to store hydrogen per unit volume. On the other hand, the volumetric density of $NaClH_6$ and $KClH_6$ is decreased owing to the larger and heavier alkali atoms. Therefore, the effectiveness of hydrogen storage in perovskite hydrides is greatly influenced by the introduction of heavier atoms at the A-site of the material. Graphical demonstrations for the volumetric densities for $LiClH_6$, $NaClH_6$, and $KClH_6$ are portrayed in Fig. 2(c).

Elastic constants and mechanical characteristics

Elastic properties of the crystal are mostly determined by elastic constants, which characterize how a material reacts to outside

Table 2 Solid state hydrogen storage for $XClH_6$ (X = Li, Na, and K)

Perovskite	Gravimetric density (wt%)	Desorption temperature (K)	Volumetric density (gH_2 L^{-1})
$LiClH_6$	10.97	538.06	43.91
$NaClH_6$	8.39	461.37	40.41
$KClH_6$	6.92	446.52	37.61

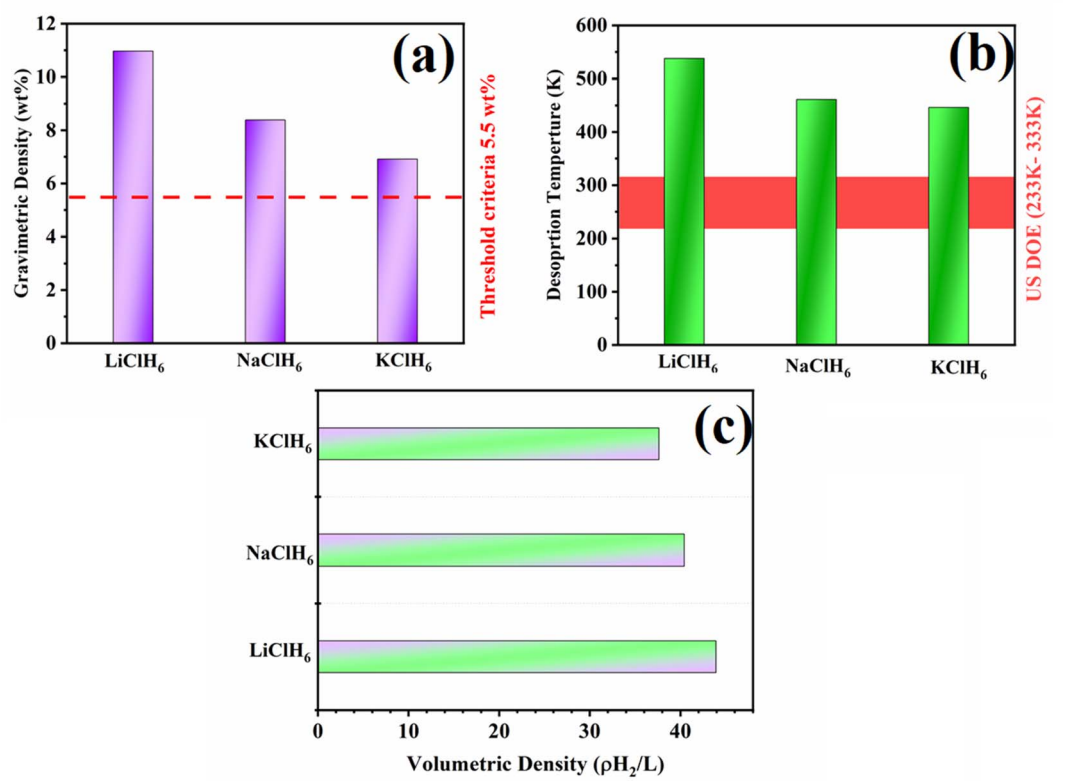

Fig. 2 (a) Gravimetric ratio, (b) desorption temperature and (c) volumetric density for $XClH_6$ (X = Li, Na, and K).

forces. These values offer important details regarding the mechanical strength and stability of the compound.[42] By computing the stress tensor components during microscopic deformation, the elastic constants were established at zero pressure, guaranteeing volume retention throughout lattice distortion.[43] The second derivative of stress tensors was employed to calculate the elastic properties for $XClH_6$ (X = Li, Na, and K). As the structural properties reveal that the structures are of cubic symmetry, the elastic constants shrink to C_{11}, C_{12}, and C_{44}. Thomas Charpin's approach is used to attain these three elastic constants. The uniaxial strains in the materials are assessed *via* C_{11}; the shear coupling between perpendicular axes is addressed *via* C_{12}, whereas C_{44} describes the shear deformation occurring in the material under the influence of external strains.[44] These elastic constants indicate a deteriorating pattern as the composition of the studied hydrides is varied from "Li" to "K". All the computed elastic parameters and the mechanical properties for $LiClH_6$, $NaClH_6$, and $KClH_6$ are listed in Table 3. The material's resistance to uniform compression is described *via* the bulk modulus.[45] The calculated values of the bulk modulus show that $LiClH_6$ has a slightly higher value in comparison with $NaClH_6$ and $KClH_6$, which signifies that it possesses a slightly higher resistance towards uniform compression. The shear modulus illustrates the material's resistance to twisting and bending in the presence of external forces. Shear modulus for solid materials is usually computed using Voigt and Reuss approximations.[46] The computed shear modulus values for the studied hydrides report a declining

Table 3 Elastic properties of $XClH_6$ (X = Li, Na, and K) computed *via* the Thomas Charpin's technique

Parameters	$LiClH_6$	$NaClH_6$	$KClH_6$
C_{11} (GPa)	45.3	38.79	29.14
C_{12} (Gpa)	11.2	9.56	5.42
C_{44} (Gpa)	16.7	13.3	8.31
B (Gpa)	22.5	19.30	13.3
G (Gpa)	16.8	13.8	9.58
Y (Gpa)	40.4	33.4	23.1
A	0.92	0.91	0.70
B/G	1.34	1.39	1.40
ν	0.20	0.21	0.21
C_{12}–C_{44} (Gpa)	−5.5	−3.74	−2.89
H_v (Gpa)	3.36	2.66	1.84
μ_m	1.34	1.45	1.60
v_l (m s^{-1})	7165.11	5933.25	4709.54
v_t (m s^{-1})	4382.13	3590.32	2853.65
v_m (m s^{-1})	4838.43	3968.44	3153.76
θ_D (K)	547.6	436.11	331.933
$T_m = 553 + (5.91 \times C_{11}) \pm 300$ (K)	820.72	782.24	725.21

trend, which implies that as the composition of the hydride is altered by introducing alkali earth metals with higher atomic masses, the material's opposition to twisting and turning declines. The material's capacity to withstand changes in the elongation of the material is defined through the Young's modulus.[47] Among the studied hydrides, the computed Young's modulus implies that $LiClH_6$ is highly resistant to change in the material's length. The anisotropy factor, which reflects how

a material behaves under different loading situations, characterizes how much a material's elastic constants depend on the direction of stress or strain. For the standard limit, $A = 0$ or $A = 1$, the materials are considered to be independent of the directions of stress and strain applied, which gives rise to an isotropic material, whereas higher or lower values of the anisotropic factor to the standard limit result in an anisotropic material.[48] From the obtained value of the anisotropy factor for the studied hydrides, it is observed that $LiClH_6$ and $NaClH_6$ indicate a higher tendency of being isotropic, whereas for $KClH_6$, an anisotropic nature is observed. The assessment of the material's ductile or brittle behavior is crucial, as these properties can help in classifying materials suitable for use in industrial applications and energy storage devices. To determine whether the studied hydrides are brittle or ductile, we assessed different parameters. The numerical value that aids in assessing the ductile or brittle nature of a material is 1.75. When B/G > 1.75, the compound possesses a higher tendency to endure plastic deformation, whereas for B/G < 1.75, the compound possesses a lower tendency to endure plastic deformation.[49] The evaluated B/G values for $LiClH_6$, $NaClH_6$, and $KClH_6$ are lower than 1.75, indicating that these materials possess a lower tendency to endure plastic deformation and can break under minimum stress. Poisson's ratio reports a numerical value of 0.26, which is the transition value that helps in identifying ductile and brittle behavior of materials. For $\nu > 0.26$, the material becomes ductile, and for $\nu < 0.26$, the material is termed brittle. From the computed values of (ν), it is reported that all three studied hydrides are brittle compounds. The criteria mentioned for brittle materials according to Cauchy's pressure are that the difference between C_{12} and C_{44} should be negative.[50] The evaluated difference between C_{12} and C_{44} for all three hydrides is negative, which implies that the studied hydrides are brittle. The material's resilience towards localized plastic deformation is assessed *via* its overall hardness, especially when subjected to pressing, sliding, or scratching.[51] From the evaluated results, it is noticed that different cation combinations at the A-site have significantly reduced the hardness value. The effectiveness of material removal during machining is connected to the machinability index.[52] A higher index allows for the removal of more material more quickly without sacrificing the cut quality. Among the studied hydrides, $KClH_6$ possesses an upper machinability index value, which proposes that less machinery effort is required to mold this material as compared to $LiClH_6$ and $NaClH_6$. Given that the specified velocities correlate to various kinds of elastic waves propagating through each material, these materials are most likely hydrides or complexes incorporating alkali metal chlorides. $LiClH_6$ exhibits the maximum longitudinal wave velocity at 7165.11 m s^{-1}, followed by $KClH_6$ and $NaClH_6$, which have gradually lower velocities of 4709.54 m s^{-1} and 5933.25 m s^{-1}, respectively. Compared to the other two materials, this pattern implies that $LiClH_6$ is more resistant to deformation under compressive stress, which is usually a sign of a denser or more rigid material structure. With $LiClH_6$ having the maximum velocity at 4382.13 m per s and $KClH_6$ having the lowest at 2853.65 m s^{-1}, the transverse wave velocity also exhibits the same declining pattern. The material's shear resistance is indicated by the transverse wave velocity, and the data indicate that $LiClH_6$ has the highest shear stiffness. $LiClH_6$ once again displays the greatest value, 4838.43 m s^{-1}, followed by $NaClH_6$ and $KClH_6$ with progressively decreasing values. This pattern is consistent with the mixed wave velocity, which normally represents the combined effects of longitudinal and transverse wave propagation. These results demonstrate how these three materials differ in terms of their mechanical characteristics and elastic behavior, with $LiClH_6$ continuously exhibiting better elastic qualities than $NaClH_6$ and $KClH_6$. One measure used to describe a solid's vibrational characteristics is the Debye temperature.[53] It has to deal with the maximum energy phonon (quantized lattice vibrations) that the material is capable of having. $LiClH_6$ is stiffer than $NaClH_6$ and $KClH_6$ because a higher value denotes stiffer bonds and stronger atomic interactions. Assessing the melting temperature is essential to analyzing the material's thermal stability.[54] The formula that represents the elastic stiffness constant is used for its calculation. Higher values indicates better thermal stability, as seen in $LiClH_6$ compared to the others, which implies that it can endure a high amount of external heat without compromising its thermal stability.

Electronic properties

Electrical characteristics of a solid material, which control its basic interactions and capabilities, can be used to understand its nature. Its electrical conductivity and optical absorbance are determined by the electronic band gap.[55] The efficiency of electron and hole motion under an electric field is revealed by charge carrier mobility. Together, these characteristics aid in determining the material's viability for applications in energy-related technologies, electronics, and photonics. The electronic structures for $XClH_6$ (X = Li, Na, and K) are analyzed using mBJ. The energy dispersion curves for all studied hydrides are obtained across the same high symmetry points. The Fermi level acts as a boundary that separates the occupied states from the unoccupied states. For the studied hydrides, indirect bandgaps are noticed, revealing that these hydrides are semiconductors. For $LiClH_6$, $NaClH_6$, and $KClH_6$, the bandgaps are noted at 0.29 eV, 0.55 eV, and 1.87 eV, respectively, as shown in Fig. 3. An increase in the bandgap value is seen as the A-site is replaced from "Li" to "K," which implies that the substitution of a heavier atom at the A-site in the material can significantly enhance the material's bandgap, leading to different physical properties. It is also noticeable that substantial changes are seen in the conduction band with A-site substitution, whereas slight variations are noticed in the energy states in the valence band for all studied hydrides. The obtained results from the band structure profiles can also be noticed from the TDOS, which are also given in Fig. 3. From the total density of state plots, it is noticed that with A-site substitution from "Li" to "K," the number of available energy states increases. The contributions from the individual orbitals (s, p, d, f) can be analyzed by evaluating the PDOS. In $LiClH_6$, maximum contributions are noticed from the "s" orbital of the hydrogen atom in the valence

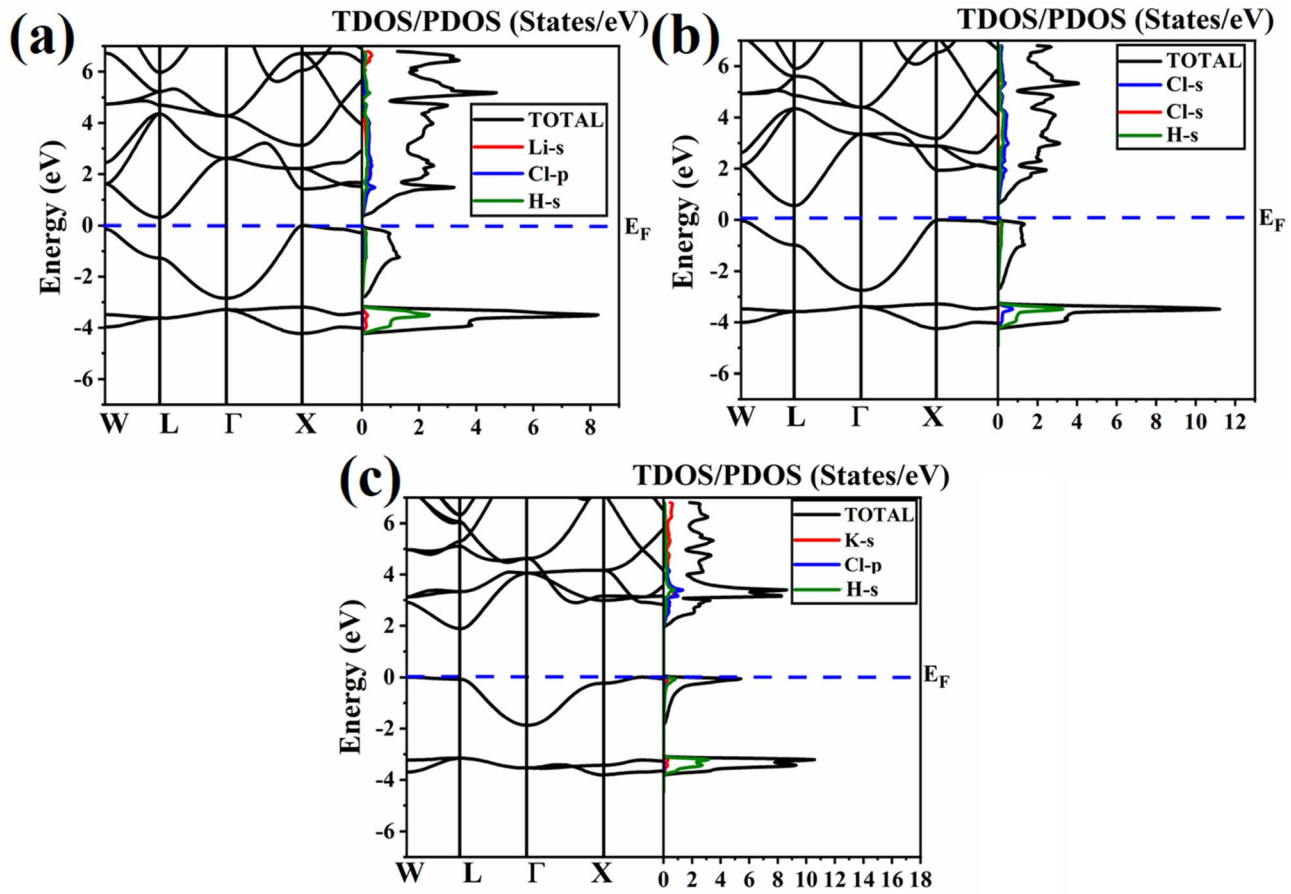

Fig. 3 Electronic properties for (a) $LiClH_6$, (b) $NaClH_6$ and (c) $KClH_6$.

band, whereas the Cl-p and Li-s states showed significant contributions in the conduction band. Hybridization of Cl-s, Cl-p, and H-s is noticed in the conduction band, whereas maximum contributions are noticed from the H-s state in the valence band in $NaClH_6$. In $KClH_6$, hybridization of K-s, Cl-p, and H-s is noticed in the conduction band, whereas in the valence band, H-s indicates higher dominance.

Optical properties

A material's suitability for optoelectronic applications is largely determined by its optical characteristics, which specify how it interacts with electromagnetic radiations. These characteristics are described by the dielectric function, which defines the interaction between photons and the material's electrons and explains the material's linear response to incident electromagnetic waves. Advanced formulas like the Ehrreich and Cohen equations are used to investigate the optical properties of complicated materials.[56] The optical characteristics for $XClH_6$ (X = Li, Na, and K) are computed from 0 to 8 eV energy. The divergence of light and the dispersion power of the material are assessed through the real part $\varepsilon_1(\omega)$ of the dielectric equation.[57] The $\varepsilon_1(\omega)$ for $XClH_6$ (X = Li, Na, and K) is displayed in Fig. 4(a). At zero energy, the static values for $LiClH_6$, $NaClH_6$, and $KClH_6$ are noticed as 5.33, 7.52, and 8.93. These static values are obtained through Penn's model, which is mathematically stated as $\varepsilon_1(0) = \left(\frac{h\omega_p}{E_g}\right)^2 + 1$, in which $\varepsilon_1(0)$ is inversely linked to the electronic bandgap of the material. The maximum values of the real part for $LiClH_6$, $NaClH_6$, and $KClH_6$ are observed at 1.61 eV, 1.71 eV, and 2.19 eV. Weak polarization is also observed for all three hydrides in the UV region. Among all the studied hydrides, $LiClH_6$ reports the highest polarization and dispersion of the incident light in the visible range. The $\varepsilon_2(0)$ indicates the material's tendency to absorb the incident electromagnetic radiation,[58] and for the studied hydrides, it is plotted in Fig. 4(b). For all studied hydrides, no absorption is described when the energy is increased to 1 eV. Strong absorption peaks are seen in the visible region for $LiClH_6$, $NaClH_6$, and $KClH_6$ at 1.78 eV, 2.05 eV, and 3.3 eV, whereas a weak absorption is also noticed for all three hydrides in the UV region. From the $\varepsilon_2(0)$ plots, it is noticed that $LiClH_6$ has a higher capacity to absorb visible radiation compared to $NaClH_6$ and $KClH_6$. The tendency of the material to refract or bend the incident light when it transitions between two media is measured *via* the refractive index. The plot of $n(\omega)$ for $XClH_6$ (X = Li, Na, and K) is shown in Fig. 4(c). The static values of the refractive index are computed using the mathematical relation as $n(0) = \sqrt{\varepsilon_1(0)}$, which implies that the real part and refractive index are interlinked.

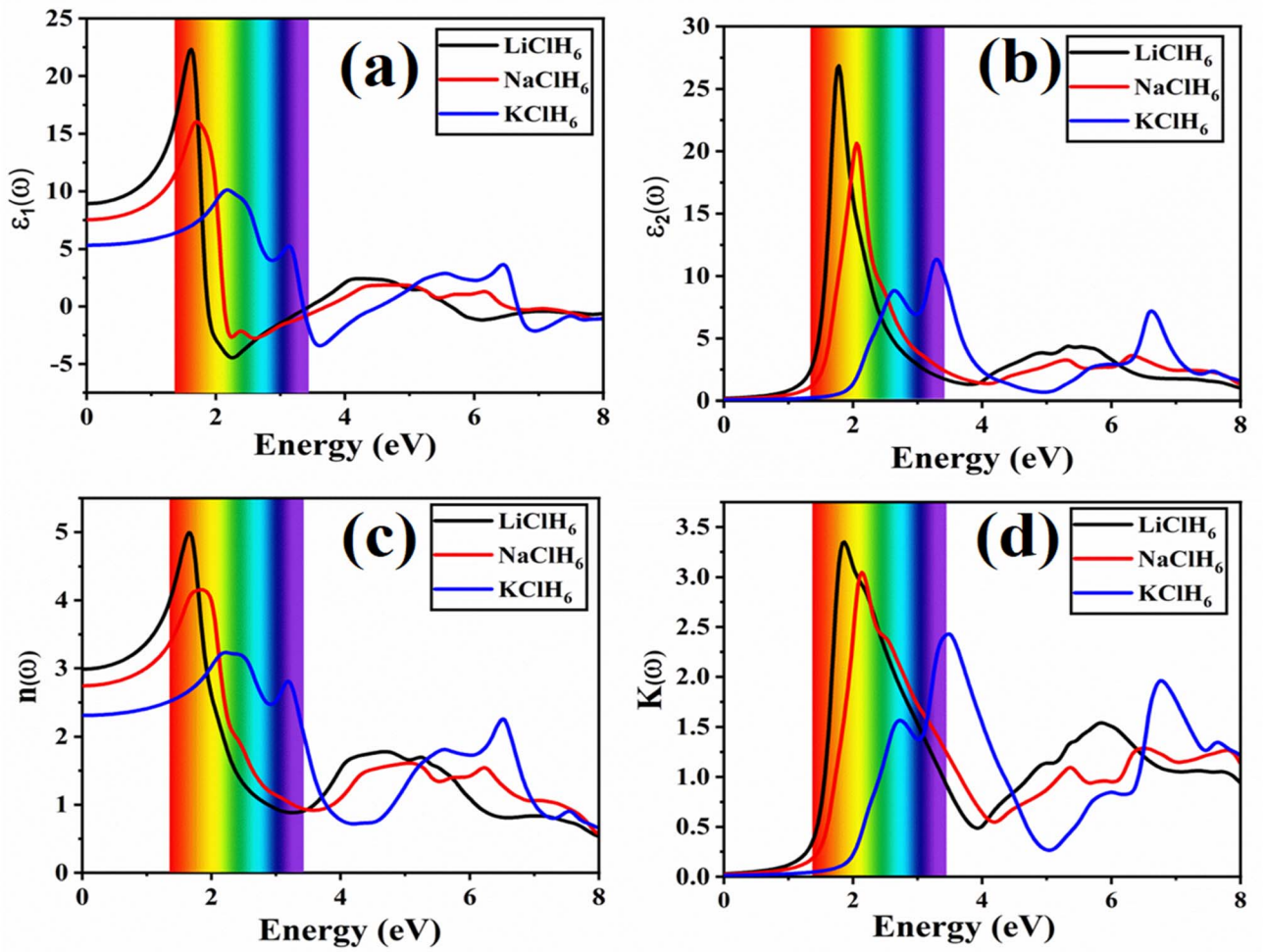

Fig. 4 The real (a) and imaginary (b) epsilon, refractive index and extinction coefficient of $XClH_6$ (X = Li, Na, and K).

The static refractive index is obtained as 2.98, 2.74, and 2.30 for $LiClH_6$, $NaClH_6$, and $KClH_6$, respectively. The highest values of $n(\omega)$ for $LiClH_6$, $NaClH_6$, and $KClH_6$ are reported in the visible region at 1.67 eV, 1.86 eV, and 2.24 eV, respectively, which depict that the refractive index can be adjusted and the material can be optimized for applications aiming at particular visible wavelengths by changing the composition. Moreover, these hydrides indicate potential suitability for optoelectronic devices, including lenses, filters, or coatings, that are tailored for particular wavelengths within this energy range, as highlighted by the reported refractive index values in the visible range. The extinction coefficient helps predict the losses caused by the material to the incident radiation, and for $LiClH_6$, $NaClH_6$, and $KClH_6$, it is shown in Fig. 4(d). The extinction coefficient reports the largest attenuation in the visible range at 1.86 eV, 2.13 eV, and 3.49 eV, respectively, for $LiClH_6$, $NaClH_6$, and $KClH_6$.

Optical conductivity highlights a material's function in photon–matter interactions by indicating how well it absorbs energy from incident electromagnetic waves and transforms it into heat or electrical excitation. For $LiClH_6$, $NaClH_6$, and $KClH_6$, the calculated optical conductivity is shown in Fig. 5(a). The highest peaks of optical conductivities for $LiClH_6$ and $NaClH_6$ are noticed in the visible region at 1.78 eV and 2.08 eV, whereas for $KClH_6$, the highest optical conductivity peak is noticed in the UV region at 6.62 eV. A major peak of optical conductivity is also noticed in the visible region at 3.3 eV for $KClH_6$. The studied hydrides are reported to be an efficient absorber in the visible spectrum because of their high optical conductivity, which shows that electromagnetic energy is being efficiently dissipated into electronic excitations. The percentage of electromagnetic radiation that bounces off a material's surface is known as its reflectivity. It is computed as a percentage or dimensionless ratio. At zero energy, the static reflectivity values are observed as 0.24, 0.21, and 0.15, respectively, for $LiClH_6$, $NaClH_6$, and $KClH_6$. The highest reflectivity peaks for $LiClH_6$, $NaClH_6$, and $KClH_6$ are reported at 1.89 eV, 2.19 eV, and 3.65 eV, as depicted in Fig. 5(b). With the enhancement in photon energy, the reflectivity plots for $LiClH_6$, $NaClH_6$, and $KClH_6$ report significant reflectance in the UV region. The absorption coefficient for $LiClH_6$, $NaClH_6$, and $KClH_6$ is presented in Fig. 5(c). The studied hydrides show significant absorption peaks in the visible region. For $LiClH_6$, $NaClH_6$, and KClH6, the peaks in the visible region are 1.89 eV,

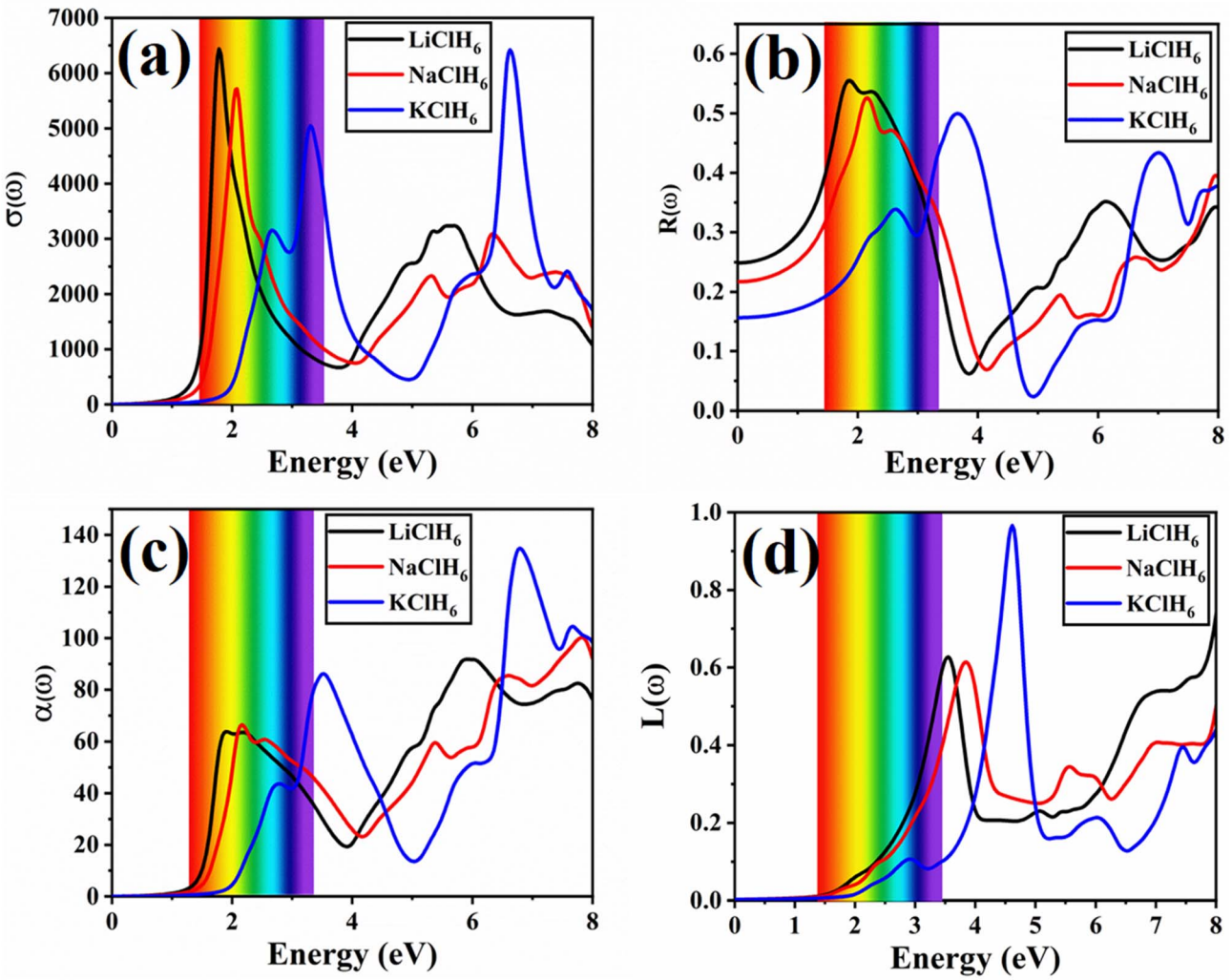

Fig. 5 Optical conductivity (a), reflectivity (b), absorption (d) and energy loss (d) of $XClH_6$ (X = Li, Na, and K).

2.16 eV, and 3.49 eV, whereas the maximum peaks are observed at 5.94 eV, 7.87 eV, and 6.78 eV. The way that particles, waves, or fields disperse energy when they interact with a material is designated by the energy loss $L(\omega)$ function. The $L(\omega)$ peaks for $LiClH_6$, $NaClH_6$, and $KClH_6$ are noticed at 3.57 eV, 3.85 eV, and 4.61 eV, respectively, as shown in Fig. 5(d). Among the studied hydrides, it is observed that $KClH_6$ reports the maximum loss as compared to $LiClH_6$ and $NaClH_6$.

Conclusion

A DFT-based study of cubic perovskite $XClH_6$ (X = Li, Na, and K) hydrides is presented in this work. It details each hydride's physical characteristics and hydrogen storage capacity by utilizing the Wien2K code. The quantum mechanical effects of each perovskite hydride are assessed *via* the mBJ functional. The obtained lattice parameters, ground state energies, tolerance factors, and negative values of the formation energies imply that the studied hydrides are stable and can be synthesized experimentally. The mechanical stability criteria mentioned by Born's criteria are completely fulfilled by the elastic constants of $XClH_6$ (X = Li, Na, and K). The computed parameters revealed that $LiClH_6$, $NaClH_6$, and $KClH_6$ are brittle. Thermodynamic characteristics imply that the studied hydrides have a higher tendency to endure high temperatures. Indirect bandgaps of 0.29 eV, 0.55 eV, and 1.87 eV are obtained for $LiClH_6$, $NaClH_6$, and $KClH_6$. The interaction of the studied hydrides with electromagnetic radiation depicts that the high polarization, reflectance, and optical conductivity in the visible area make them viable materials for visible optoelectronic devices. Furthermore, the evaluated high hydrogen storage ability of $LiClH_6$, $NaClH_6$, and $KClH_6$ implies that these hydrides satisfy the mentioned US DOE criteria for hydrogen applications.

Conflicts of interest

The authors have no conflicts of interest.

Data availability

All data produced are available in the manuscript. The authors have no additional data to declare.

Acknowledgements

This work was supported and funded by the Deanship of Scientific Research at Imam Mohammad Ibn Saud Islamic University (IMSIU) (grant number IMSIU-DDRSP2503).

References

1 N. Xu, Y. Chen, S. Chen, S. Li and W. Zhang, *Int. J. Hydrogen Energy*, 2024, **50**, 114–122.
2 M. Umer, G. Murtaza, N. Ahmad, A. Ayyaz, H. H. Raza, A. Usman, A. Liaqat and S. Manoharadas, *Int. J. Hydrogen Energy*, 2024, **61**, 820–830.
3 H. Murtaza, Q. Ain, S. A. Issa, H. M. Zakaly and J. Munir, *Int. J. Hydrogen Energy*, 2024, **94**, 1084–1093.
4 L. Zhu, Y. Song, H. Chen, M. Wang, Z. Liu, X. Wei, C. Zhao and T. Ai, *Int. J. Hydrogen Energy*, 2025, **101**, 161–172.
5 M. A. Rehman, Z. U. Rehman, M. Usman, S. Y. Alomar, M. J. Khan and J. Fatima, *Int. J. Hydrogen Energy*, 2024, **84**, 447–456.
6 M. K. Masood, W. Khan, K. Chaoui, Z. Ashraf, S. Bibi, A. Kanwal, A. A. Alothman and J. Rehman, *Int. J. Hydrogen Energy*, 2024, **63**, 1248–1257.
7 Y. Qin, R. Song, S. Chen, Y. Chen, J. Hou, N. Xu and W. Zhang, *Int. J. Hydrogen Energy*, 2024, **88**, 251–259.
8 Z. ur Rehman, M. A. Rehman, B. Rehman, M. Amjad, M. Awais, I. Iqbal and A. Rafique, *J. Phys. Chem. Solid.*, 2024, **186**, 111801.
9 Y. Du, N. Xu, S. Chen, Y. Chen, R. Song, W. Luo and W. Zhang, *Int. J. Hydrogen Energy*, 2024, **78**, 713–720.
10 J. Zhang, S. Chen, J. Hou, Y. Chen, J. Liu, N. Xu, R. Song and W. Zhang, *Phys. B Condens. Matter*, 2024, 416488.
11 T. Tang and Y. Tang, *Ceram. Int.*, 2024, 52270–52283.
12 N. Al-Zoubi, A. Almahmoud, A. Almahmoud and A. Obeidat, *Int. J. Hydrogen Energy*, 2024, **93**, 822–831.
13 A. Mera and M. A. Rehman, *Int. J. Hydrogen Energy*, 2024, **50**, 1435–1447.
14 R. Song, N. Xu, Y. Chen, S. Chen, S. Zhang, Y. Du and W. Zhang, *Int. J. Hydrogen Energy*, 2024, **87**, 566–573.
15 H. Benaali, S. Bahhar, A. Tahiri, Y. Didi, H. Fatihi, A. Abbassi, B. Manaut and M. Naji, *Inorg. Chem. Commun.*, 2024, 113033.
16 C. Gu, G.-H. Gao and Y.-X. Yu, *J. Chem. Phys.*, 2003, **119**(1), 488–495.
17 C. Gu, G.-H. Gao, Y.-X. Yu and Z.-Q. Mao, *Int. J. Hydrogen Energy*, 2001, **26**(7), 691–696.
18 H. Wang, B. Wang, J. Sun, Q. Pan, G. Luo, X. Tao, Y. He, J. Pfotenhauer, T. Jin and Z. Gan, *Int. J. Hydrogen Energy*, 2024, **57**, 822–843.
19 M. A. Rehman, Z. U. Rehman, M. Usman, S. Y. Alomar, M. J. Khan and J. Fatima, *Int. J. Hydrogen Energy*, 2024, **84**, 447–456.
20 Y. Song, M. K. Shahzad, S. Hussain, A. Farrukh, M. Riaz, H. Sattar, G. Khan, G. A. Ashraf, S. M. Ali and M. Alam, *Int. J. Hydrogen Energy*, 2024, **79**, 1472–1482.
21 M. Usman, N. Bibi, S. Rahman, M. A. Rehman and S. Ahmad, *Comput. Theor. Chem.*, 2024, **1240**, 114820.
22 R. Song, Y. Chen, S. Chen, N. Xu and W. Zhang, *Int. J. Hydrogen Energy*, 2024, **57**, 949–957.
23 M. A. Rahman, S. S. Islam, M. A. Rayhan, A. Kabir, M. A. Alim, J. Uddin, M. D. Albaqami, S. Mohammad, R. Haldhar and M. K. Hossain, *Int. J. Hydrogen Energy*, 2024, **80**, 725–732.
24 Z. Abbas, Z. Zafar, H. H. Raza, A. Parveen and S. F. Shaikh, *Int. J. Hydrogen Energy*, 2024, **60**, 212–228.
25 N. Xu, R. Song, J. Zhang, Y. Chen, S. Chen, S. Li, Z. Jiang and W. Zhang, *Int. J. Hydrogen Energy*, 2024, **60**, 434–440.
26 H. Shabbir, M. Usman, J. U. Rehman, D. Pan, S. M. Ali and R. Alotaibi, *J. Comput. Electron.*, 2024, **1–11**, 1238–1248.
27 M. Tahir, M. Usman, J. U. Rehman and M. B. Tahir, *Int. J. Hydrogen Energy*, 2024, **50**, 845–853.
28 M. Usman, D. Pan, M. K. Masood and C. Zhang, *Solid State Commun.*, 2024, **390**, 115600.
29 Y. Zhu, Y. Liang, Y. Pu and J. Xiong, *Int. J. Hydrogen Energy*, 2024, **71**, 239–249.
30 A. Algahtani, M. Liaqat, M. Sajjad, A. Quraishi, N. Kamolova, A. Almahri, N. Elboughdiri, A. U. Haq, R. M. Mohammed and V. Tirth, *Inorg. Chem. Commun.*, 2024, **170**, 113139.
31 A. Ayyaz, H. D. Alkhaldi, S. Saidi, H. Albalawi, O. Zayed, T. M. Al-Daraghmeh, Q. Mahmood and A. K. Alqorashi, *Mater. Sci. Semicond. Process.*, 2025, **186**, 109020.
32 M. K. Shahzad, S. Hussain, M. N. Khan, M. J. Aslam, R. M. Mohammed, V. Tirth, H. Alqahtani, A. Algahtani, T. Al-Mughanam and W. Azeem, *Sci. Rep.*, 2024, **14**(1), 25102.
33 H. Murtaza, J. Munir, Q. Ain, A. S. Aldwayyan, H. M. Ghaithan, A. A. A. Ahmed and S. M. Qaid, *J. Inorg. Organomet. Polym. Mater.*, 2024, **1–14**, 3401–3414.
34 F. A. Nelson, A. Basem, D. J. Jasim, T. E. Gber, M. T. Odey, A. F. Al Asmari and S. Islam, *Int. J. Hydrogen Energy*, 2024, **79**, 1191–1200.
35 K. Schwarz and P. Blaha, *Comput. Mater. Sci.*, 2003, **28**(2), 259–273.
36 F. Gasmi, R. Chemam, R. Graine, B. Boubir and H. Meradji, *J. Mol. Model.*, 2020, **26**, 1–9.
37 H. Murtaza, Q. ul Ain, J. Munir, H. M. Ghaithan, A. A. A. Ahmed and S. M. Qaid, *J. Mater. Sci. Eng. B*, 2024, 301–117171.
38 H. Murtaza, J. Munir, Q. Ain, A. S. Aldwayyan, I. Ali, H. M. Ghaithan, A. A. A. Ahmed and S. M. Qaid, *Mater. Sci. Eng., B*, 2024, **308**, 117547.
39 G. Surucu, A. Gencer, A. Candan, H. H. Gullu and M. R. Isik, *Int. J. Energy Res.*, 2020, **44**(3), 2345–2354.
40 H. Murtaza, J. Munir, H. M. Ghaithan, Q. ul Ain, A. A. A. Ahmed and S. M. Qaid, *Comput. Mater. Sci.*, 2024, **232**, 112674.
41 M. K. Masood, W. Khan, S. Bibi, A. Kanwal, S. Bibi, G. Noor, A. A. Alothman, J. Rehman and S. A. Shafiee, *J. Phys. Chem. Solids*, 2024, **192**, 112098.
42 H. Murtaza, J. Munir, Q. Ain, A. S. Aldwayyan, H. M. Ghaithan, A. A. A. Ahmed and S. M. Qaid, *J. Inorg. Organomet. Polym. Mater.*, 2024, 1–12.
43 H. Khan, M. Sohail, N. Rahman, R. Khan, M. Hussain, A. Ullah, A. Khan, A. Alataway, A. Z. Dewidar and H. O. Elansary, *Molecules*, 2022, **27**(16), 5264.

44 H. Murtaza, Q. Ain, J. Munir, H. M. Ghaithan, A. A. A. Ahmed, A. S. Aldwayyan and S. M. Qaid, *Inorg. Chem. Commun.*, 2024, **162**, 112206.
45 H. Murtaza, Q. Ain, J. Munir, A. S. Aldwayyan, H. M. Ghaithan, A. A. A. Ahmed and S. M. Qaid, *Mater. Sci. Semicond. Process.*, 2024, **181**, 108645.
46 H. Murtaza, Q. Ain, J. Munir, H. Ullah, H. M. Ghaithan, A. A. A. Ahmed and S. M. Qaid, *Sol. Energy*, 2024, **273**, 112502.
47 H. Murtaza, Q. Ain, J. Munir, H. M. Ghaithan, M. Ali, A. A. A. Ahmed and S. M. Qaid, *J. Phys. Chem. Solids*, 2024, **190**, 111934.
48 S. M. Qaid, H. Murtaza, Q. ul Ain, H. M. Ghaithan, A. A. A. Ahmed, M. Alkadi and J. Munir, *Phys. B*, 2023, **671**, 415416.
49 H. Murtaza, Q. Ain, J. Munir, H. M. Ghaithan, A. A. A. Ahmed and S. M. Qaid, *ECS J. Solid State Sci. Technol.*, 2024, **13**(3), 033006.
50 H. Murtaza, Q. Ain, J. Munir, H. M. Ghaithan, A. A. A. Ahmed, A. S. Aldwayyan and S. M. Qaid, *Phys. Scr.*, 2024, **99**(5), 055947.
51 H. Murtaza, Q. Ain, J. Munir, H. M. Ghaithan, A. A. A. Ahmed and S. M. Qaid, *Phys. Scr.*, 2024, **99**(10), 105927.
52 S. M. Qaid, H. Murtaza, Q. Ain, M. U. Din, H. M. Ghaithan, A. A. A. Ahmed and J. Munir, *Phys. B*, 2024, **685**, 416000.
53 H. Murtaza, J. Munir, Q. Ain, A. S. Aldwayyan, H. M. Ghaithan, A. A. A. Ahmed and S. E. Qaid, *J. Rare Earths*, 2024, DOI: **10.1016/j.jre.2024.10.010**.
54 S. M. Qaid, I. Mursaleen, Q. Ain, H. Murtaza, A. S. Aldwayyan, H. M. Ghaithan, A. A. AhmedAhmed and J. Munir, *J. Mater. Res.*, 2024, 1–12.
55 H. Murtaza, Q. Ain, J. Munir, H. M. Ghaithan, R. Sharma, A. A. A. Ahmed and S. M. Qaid, *Phys. B*, 2024, **677**, 415729.
56 S. Kumari, P. K. Kamlesh, L. Kumari, S. Kumar, S. Kumari, R. Singh, R. Gupta, M. S. Chauhan, U. Rani and A. S. Verma, *J. Mol. Model.*, 2023, **29**(6), 195.
57 H. Murtaza, Q. Ain, A. S. Jbara, J. Munir, A. S. Aldwayyan, H. M. Ghaithan, S. Dahbi, A. A. A. Ahmed and S. M. Qaid, *Opt. Quant. Electron.*, 2024, **56**(9), 1440.
58 H. Murtaza, Q. Ain, J. Munir, H. M. Ghaithan, A. A. A. Ahmed and S. M. Qaid, *Int. J. Hydrogen Energy*, 2024, **83**, 124–132.